Cell Reports, Volume *45*

Supplemental information

Fibroblast MrgprX2/B2 signaling drives hypertrophic scar fibrosis

Heng Xu, Meiying Sheng, Yuxin Jia, Yi Luo, Liyan Wu, Luxian Zhou, Zihan Wang, Jiawei Sun, Tianyi Shen, Liqin Zhou, Ting Wang, Yan Liu, Jing Feng, and Yixin Zhang

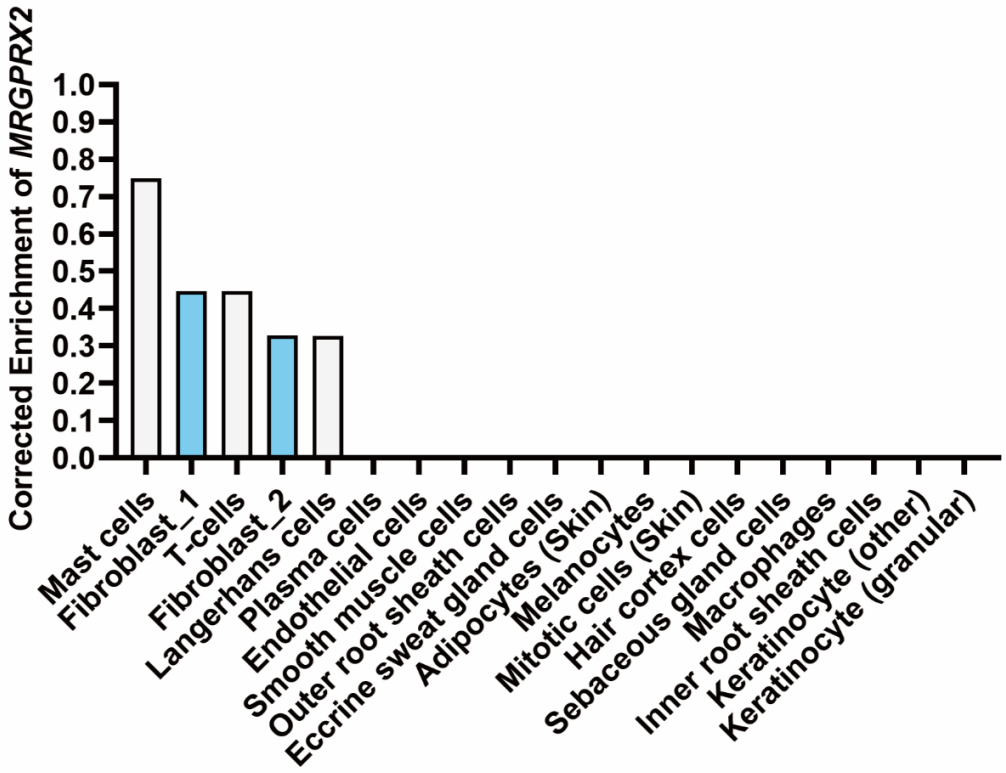

Figure S1. *MRGPRX2* expression in different cell types in human skin. Human Protein Atlas dataset showing *MRGPRX2* expression in normal skin fibroblasts. Available from: Human Protein Atlas Dataset (https://www.proteinatlas.org/).

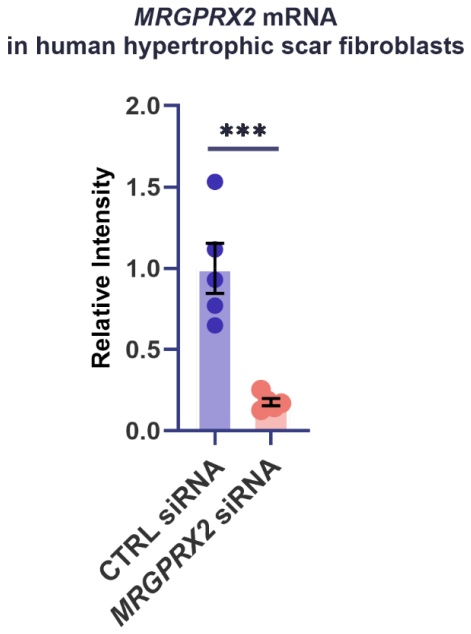

Figure S2. Validation of siRNA-mediated knockdown of *MRGPRX2* in fibroblasts derived from human hypertrophic scar tissues. n = 5 per group. Student's *t*-test.
Data are presented as mean ± SEM. ***$P < 0.001$.

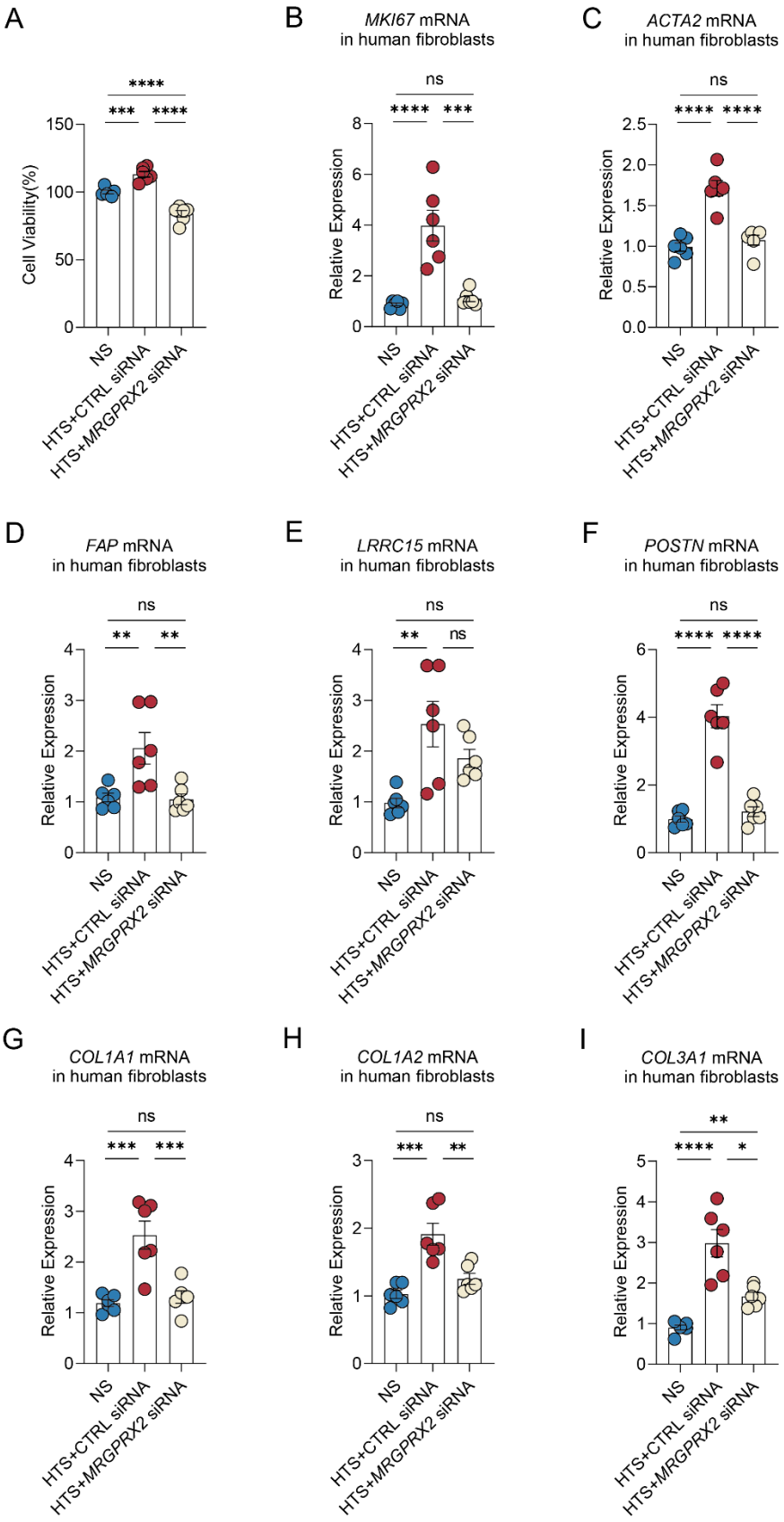
A
Cell Viability(%)
150
100
50
0
****
***
****
NS
HTS+CTRL siRNA
HTS+MRGPRX2 siRNA
B
MKI67 mRNA
in human fibroblasts
Relative Expression
8
6
4
2
0
ns
****
***
C
ACTA2 mRNA
in human fibroblasts
2.5
2.0
1.5
1.0
0.5
0.0
D
FAP mRNA
in human fibroblasts
**
**
E
LRRC15 mRNA
in human fibroblasts
**
ns
F
POSTN mRNA
in human fibroblasts
6
4
2
0
G
COL1A1 mRNA
in human fibroblasts
H
COL1A2 mRNA
in human fibroblasts
I
COL3A1 mRNA
in human fibroblasts
*

Figure S3. *MRGPRX2* drives the pro-fibrotic program in hypertrophic scar fibroblasts.
(A) Cell proliferation of human normal skin fibroblasts (NS) and hypertrophic scar fibroblasts (HTS) was assessed by CCK-8 assay following stimulation with the MrgprX2 agonist PAMP12 (50 nM). HTS were transfected with either a control siRNA or an *MRGPRX2*-targeting siRNA prior to stimulation.
(B-I) Relative mRNA expression levels of the fibrotic markers *MKI67* (B), *ACTA2* (C), *FAP* (D), *LRRC15* (E), *POSTN* (F), *COL1A1* (G), *COL1A2* (H), *COL3A1* (I) were determined by qRT-PCR in NS, HTS + CTRL siRNA, and HTS + *MRGPRX2* siRNA after PAMP12 (50 nM) treatment (n = 6 per group). One-way ANOVA with Tukey's multiple comparison test.
Data are presented as mean ± SEM. of three independent experiments. ns: not significant. $^{**}P < 0.01$, $^{***}P < 0.001$, $^{****}P < 0.0001$.

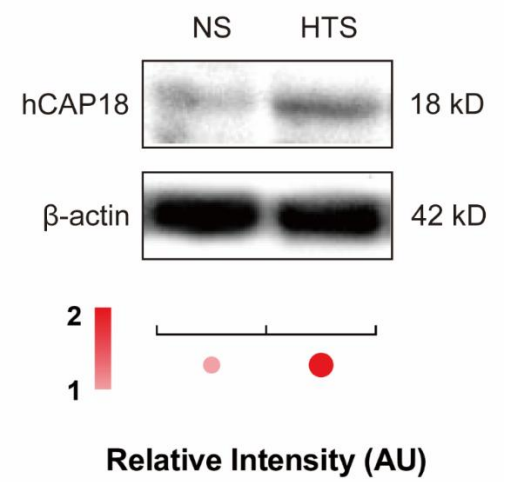

Figure S4. Western blot analysis of hCAP18 expression in fibroblasts.
Heatmap representing the expression levels of hCAP18 in normal skin and hypertrophic scar tissue groups. n = 3 per group.

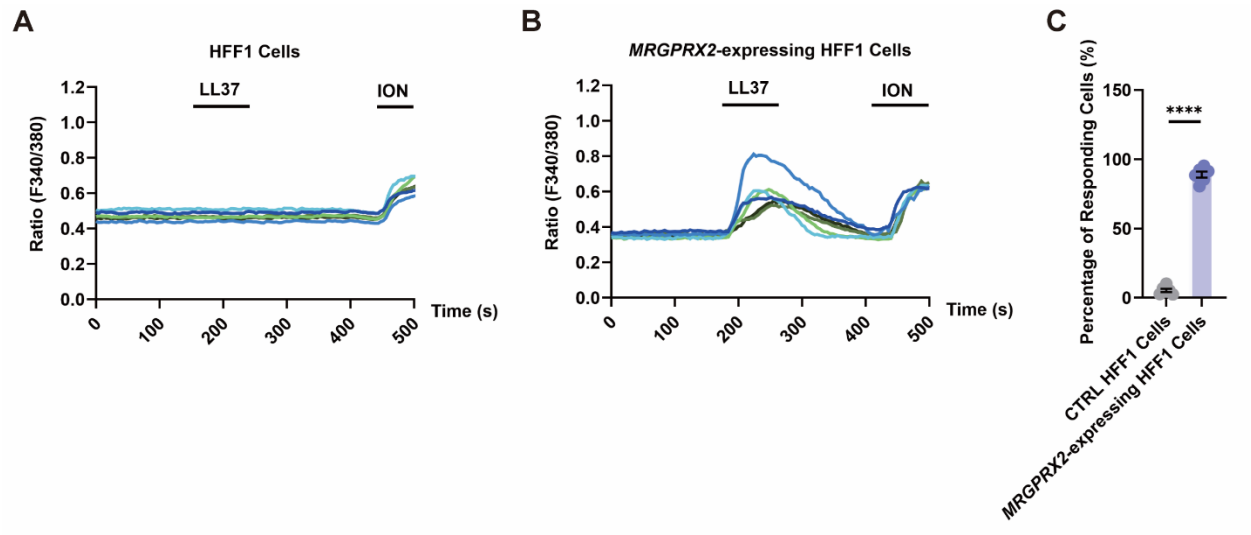

Figure S5. LL37 evokes MrgprX2-dependent calcium responses in Human foreskin fibroblasts.
(A-B) Representative $[Ca^{2+}]_i$ imaging of (A) parental HFF1 cells and (B) *MRGPRX2*-expressing HFF1 cells in response to LL37 stimulation.
(C) Quantification of calcium influx from (A-B) (n = 6 cover slips per group). Student's *t*-test.
Data are presented as mean ± SEM. ****$P < 0.0001$.

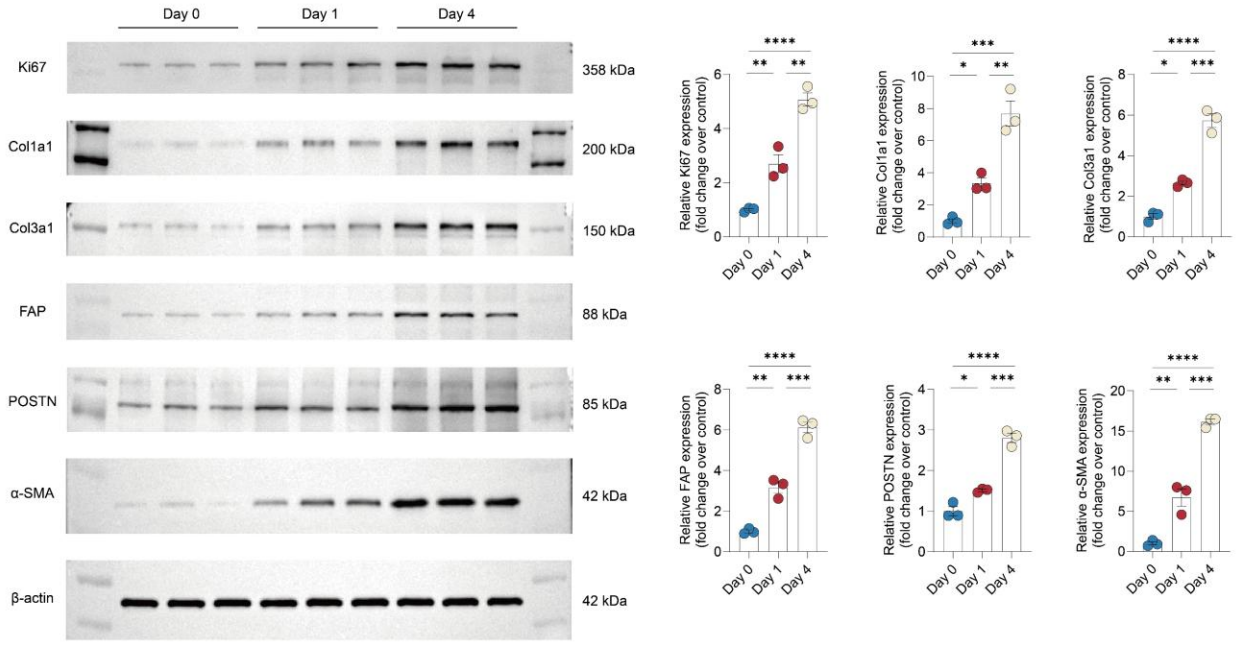

Figure S6. Time-course analysis of LL37-induced fibroblast activation and fibrotic markers in humanized skin organoids.

Representative Western blot images showing the protein levels of α-SMA, Col1a1, Col3a1, FAP, POSTN, and Ki67 in LL37-treated humanized skin organoids at Day 0, Day 1, and Day 4 post-wounding with quantitative analysis (n = 3 per group). One-way ANOVA with Tukey's multiple comparison test.

Data are shown as mean ± SEM. **P* < 0.05, ***P* < 0.01, ****P* < 0.001, *****P* < 0.0001.

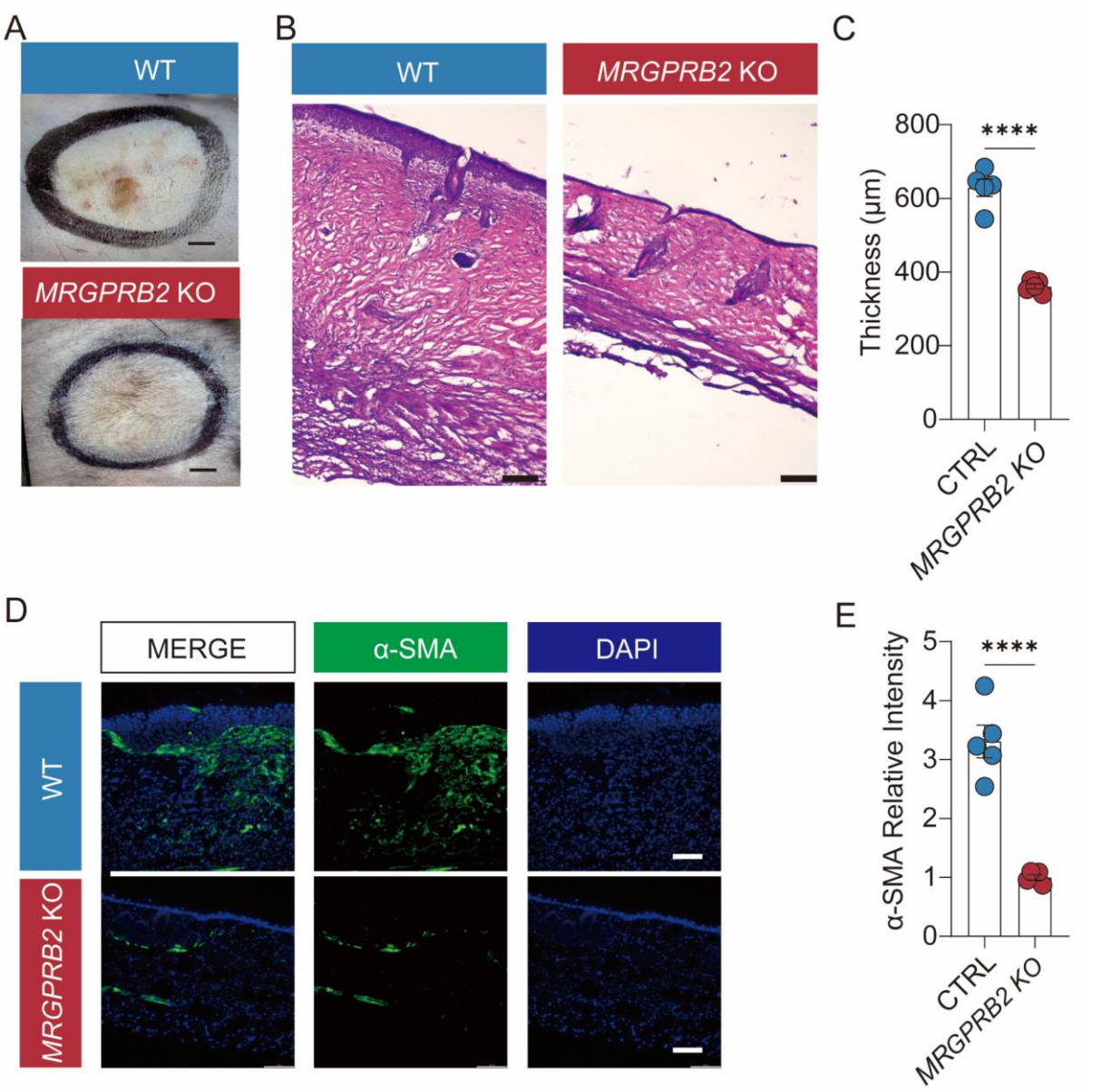

Figure S7. LL37-induced skin fibrosis is alleviated in *MRGPRB2* knockout mice.
(A) Representative gross images of skin lesions in wild-type and *MRGPRB2* knockout mice after LL37 treatment. Scale bar = 2.5 mm.
(B-C) H&E staining of skin sections and quantification of dermal thickness. Scale bar = 100 μm. Student's *t*-test.
(D-E) Immunofluorescence staining of α-SMA (D) with corresponding quantification of fluorescence intensity (E). Scale bar = 100 μm. Student's *t*-test. n=5 per group.
Data are shown as mean ± SEM. ****$P < 0.0001$.

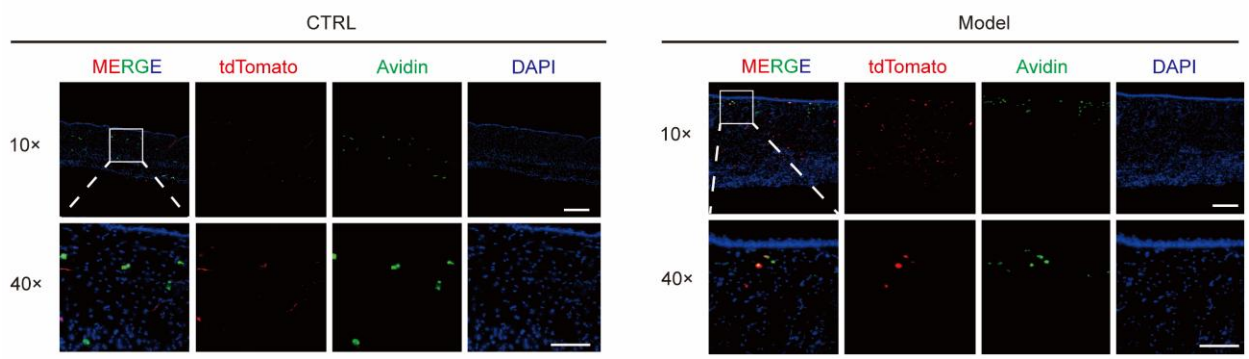

Figure S8. Representative images of skin sections from *MRGPRB2^{cre}; Ai9* mice.
Sections were co-stained with Avidin to label mast cells, showing tdTomato^{+} MrgprB2-expressing cells (n = 5 per group). Scale bars: 250 μm (10×), 100 μm (40×).

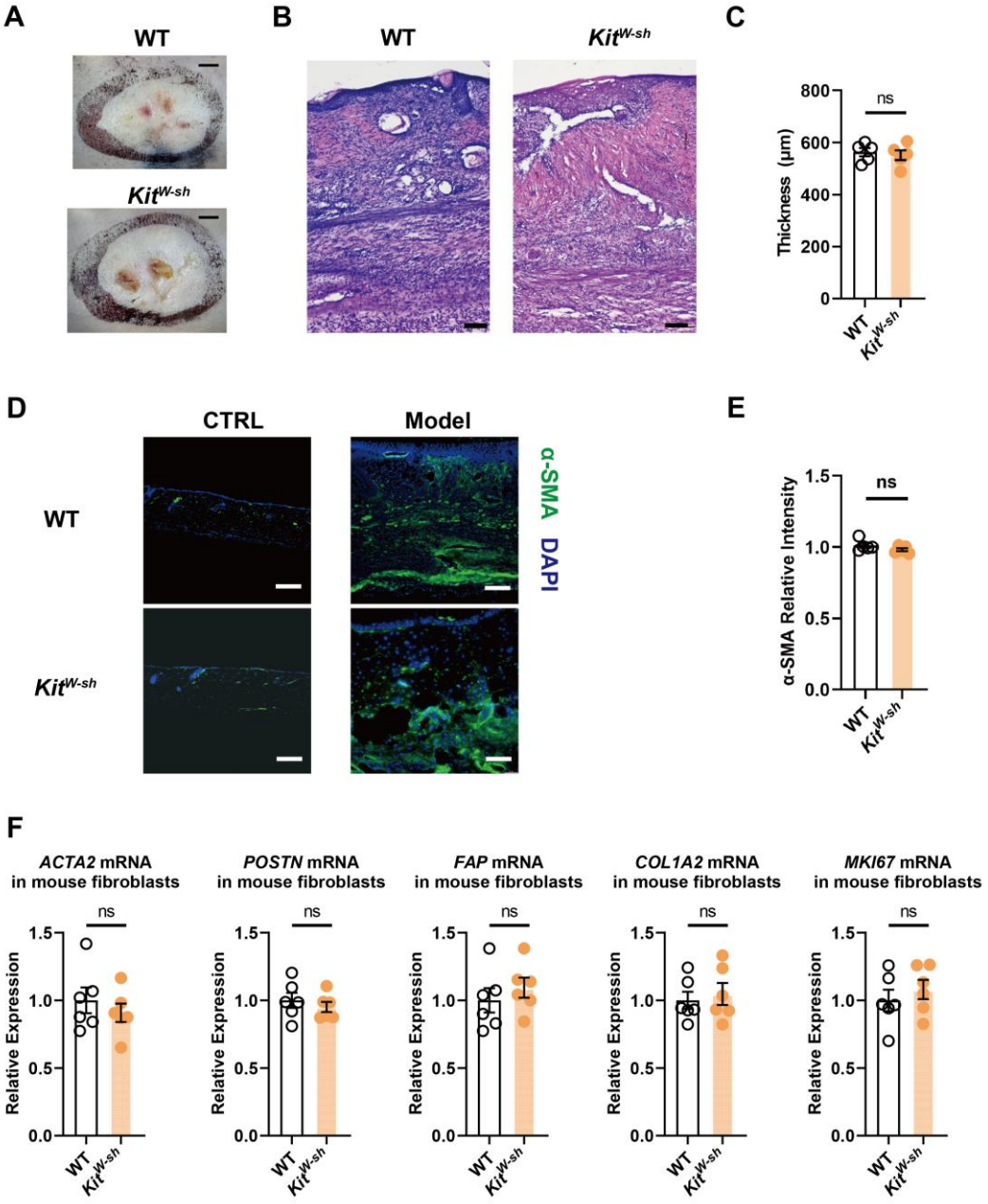

Figure S9. LL37-induced skin fibrosis persists in mast cell-deficient *Kit*$^{W\text{-}sh}$ mice.
(A) Representative gross images of LL37-treated skin in *Kit*$^{W\text{-}sh}$ mice (scale bar = 2.5 mm).
(B-C) Representative images of (B) H&E staining of skin sections and (C) quantification of dermal thickness (scale bar = 100 μm). Student's *t*-test.
(D-E) Representative images of immunofluorescence staining of α-SMA and (E) quantification of fluorescence intensity (scale bar = 100 μm). Student's *t*-test. n = 5 per group.
(F) RT-qPCR analysis of *ACTA2*, *POSTN*, *FAP*, *COL1A2*, and *MKI67* using dermal fibroblasts isolated from LL37-treated WT and *Kit*$^{W\text{-}sh}$ mice (n = 6 per group). Student's *t*-test.
Data are presented as mean ± SEM. ns: not significant.

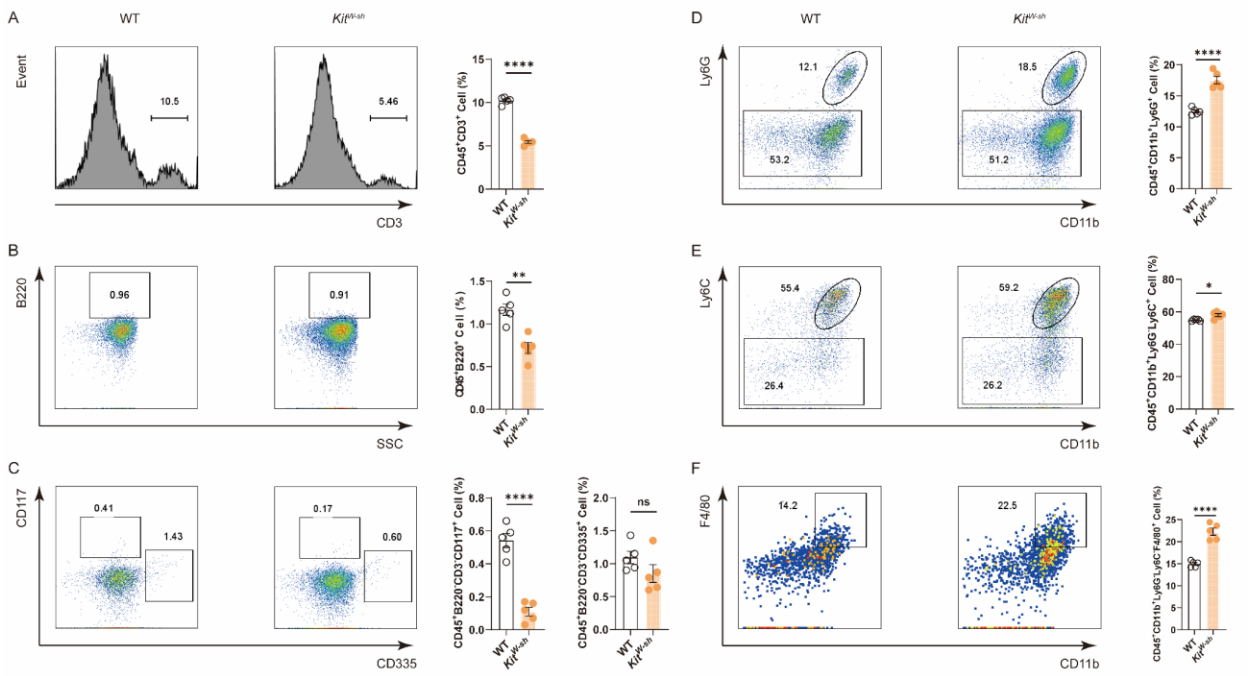

Figure S10. Mast cell depletion reduces immune cell infiltration.
(A-F) Quantification of immune cell subsets in the LL37-induced HTS-like lesions using WT and *Kit*$^{w\text{-}sh}$ mice. n = 5 mice per group
Data are shown as mean ± SEM. Student's *t*-test. ns, not significant, **P* < 0.05, ***P* < 0.01, *****P* < 0.0001.

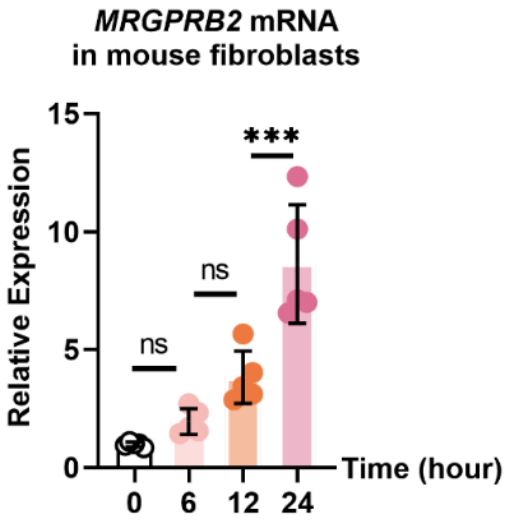

Figure S11. Time-course RT-qPCR analysis showing upregulation of *MRGPRB2* in primary mouse fibroblasts following LL37 stimulation. n = 5 per group. One-way ANOVA with Tukey's multiple comparison test.
Data are presented as mean ± SEM. ns: not significant. ****P* < 0.001.

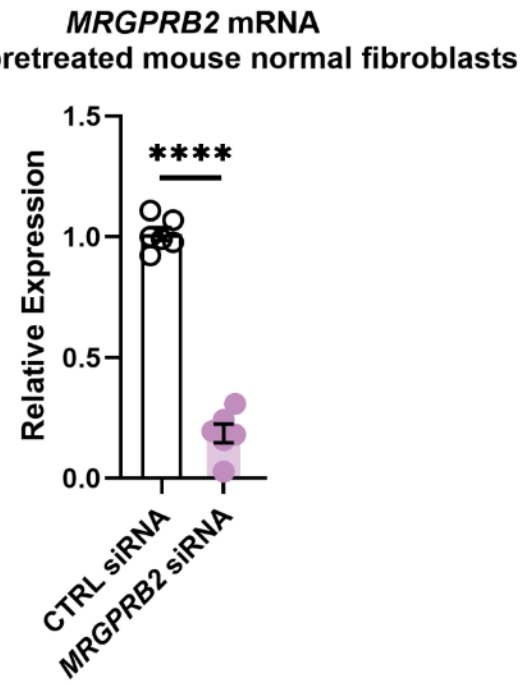

Figure S12. RT-qPCR confirming knockdown efficiency of *MRGPRB2* siRNA in LL37-treated primary fibroblasts compared to control siRNA. n = 6 per group. Student's *t*-test.
Data are presented as mean ± SEM. ****P* < 0.0001.

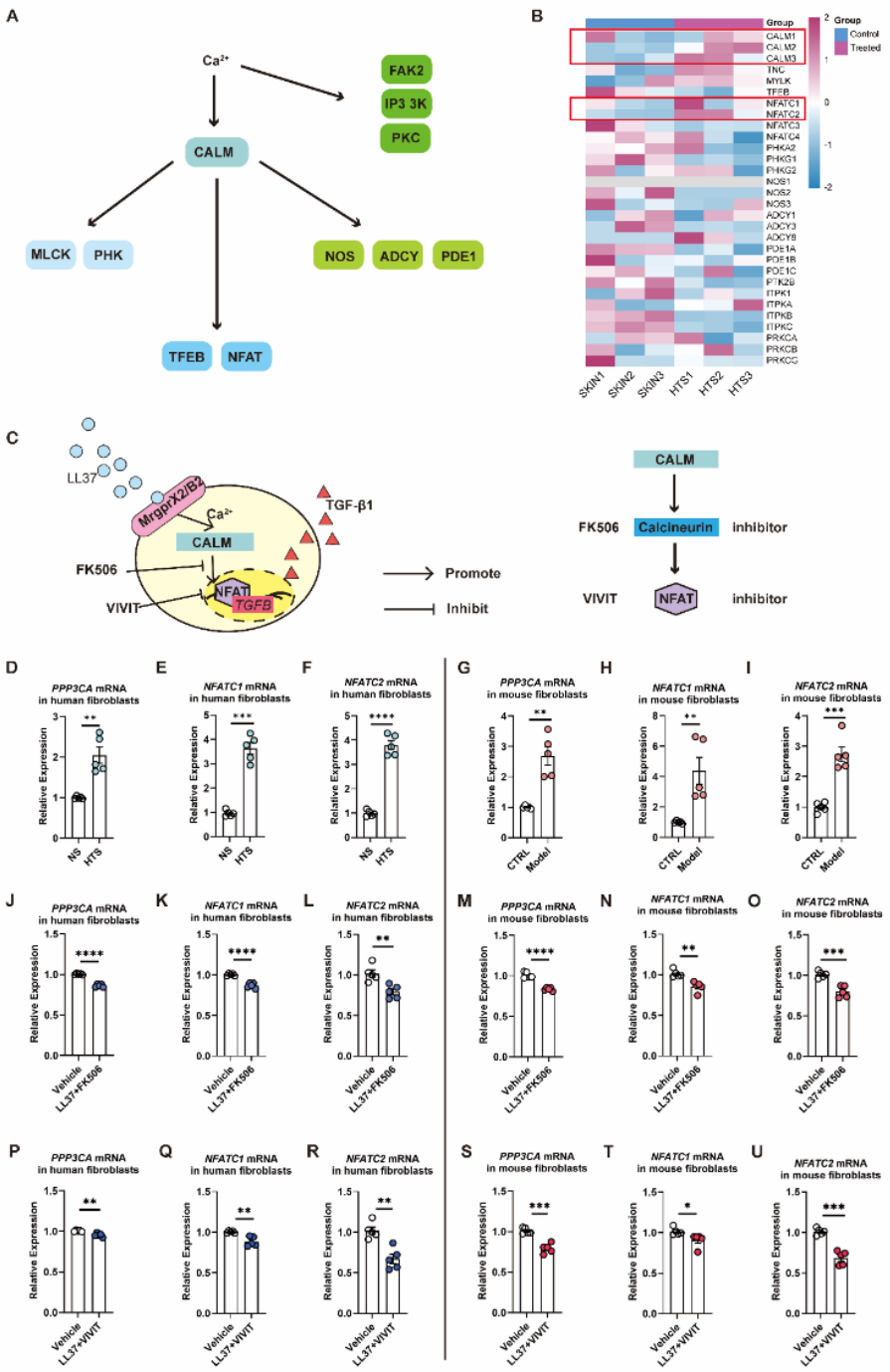

Figure S13. LL37-MrgprX2/B2 signaling activates the Ca^{2+}-calcineurin-NFAT pathway.
(A-B) Analysis of downstream signaling pathways showing (A) schematic overview of Ca^{2+}-mediated signaling and (B) heatmap of RNA-seq data highlighting upregulation of genes involved in the Ca^{2+}-calmodulin-NFAT axis in LL37-treated fibroblasts (n = 3 per group).
(C) Schematic of pharmacological intervention using FK506 (calcineurin inhibitor) and VIVIT (NFAT pathway blocker).
(D-U) RT-qPCR validation of pathway-related gene expression following LL37 stimulation and FK506/VIVIT treatment in fibroblasts (n=5 per group). Student's *t*-test.
Data are presented as mean ± SEM. **P* < 0.05, ***P* < 0.01, ****P* < 0.005, *****P* < 0.001.

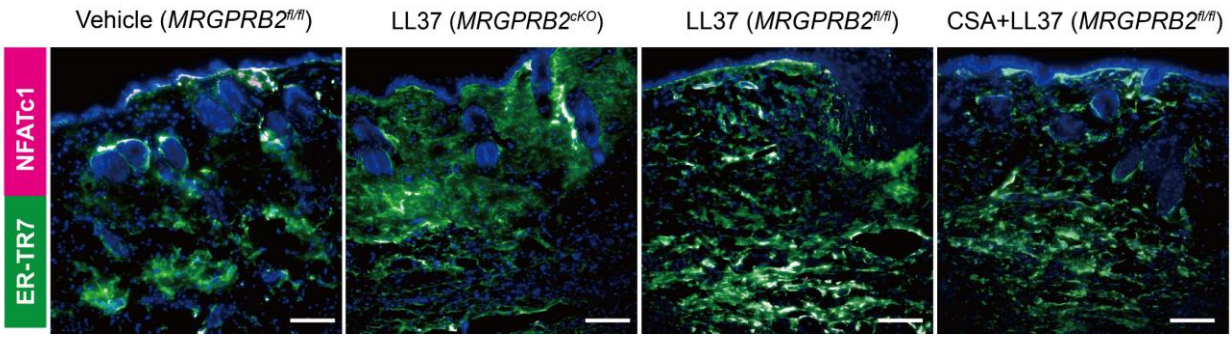

Figure S14. *MRGPRB2* is required for LL37-induced NFATc1 expression in fibroblasts.
Representative images of immunostaining for NFATc1 and ER-TR7 in skin sections. Scale bar = 25 μm.

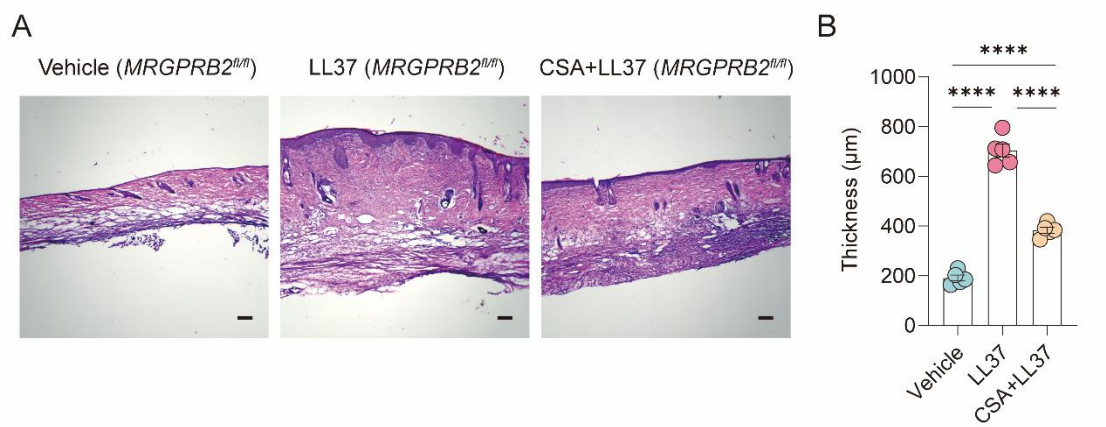

Figure S15. Pharmacological inhibition of calcineurin attenuates LL37-induced skin fibrosis.
(A) Representative H&E staining of LL37-induced HTS-like lesions. Scale bar = 100 μm.
(B) Quantification of dermal thickness. n = 5 per group. One-way ANOVA with Tukey's multiple comparison test.
Data are presented as mean ± SEM. ****$P < 0.0001$.

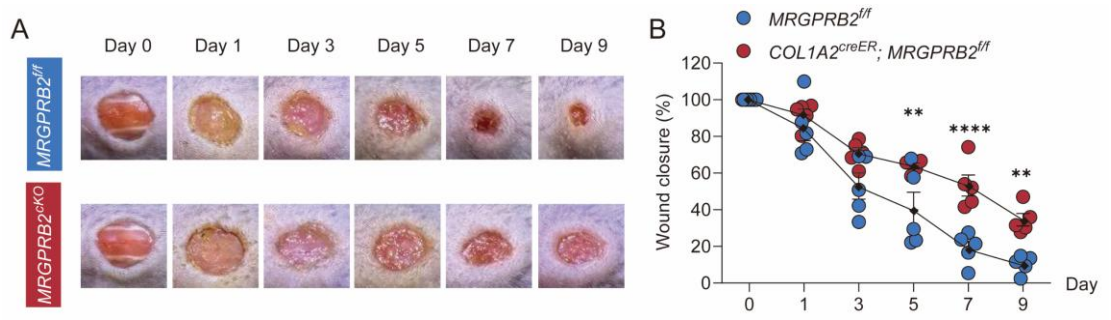

Figure S16. *MRGPRB2* in fibroblasts promotes cutaneous wound healing.
(A) Representative images of excisional wound splinting model in *MRGPRB2*$^{f/f}$ and *COL1A2*^{creER}*; MRGPRB2*$^{f/f}$ mice at days 0, 1, 3, 5, 7, and 9 post-wounding.
(B) Quantitative analysis of wound closure rate (percentage of initial wound area). n = 5 per group. Two-way ANOVA with Bonferroni's post hoc test.
Data are presented as mean ± SEM. ***P* < 0.01, *****P* < 0.0001.

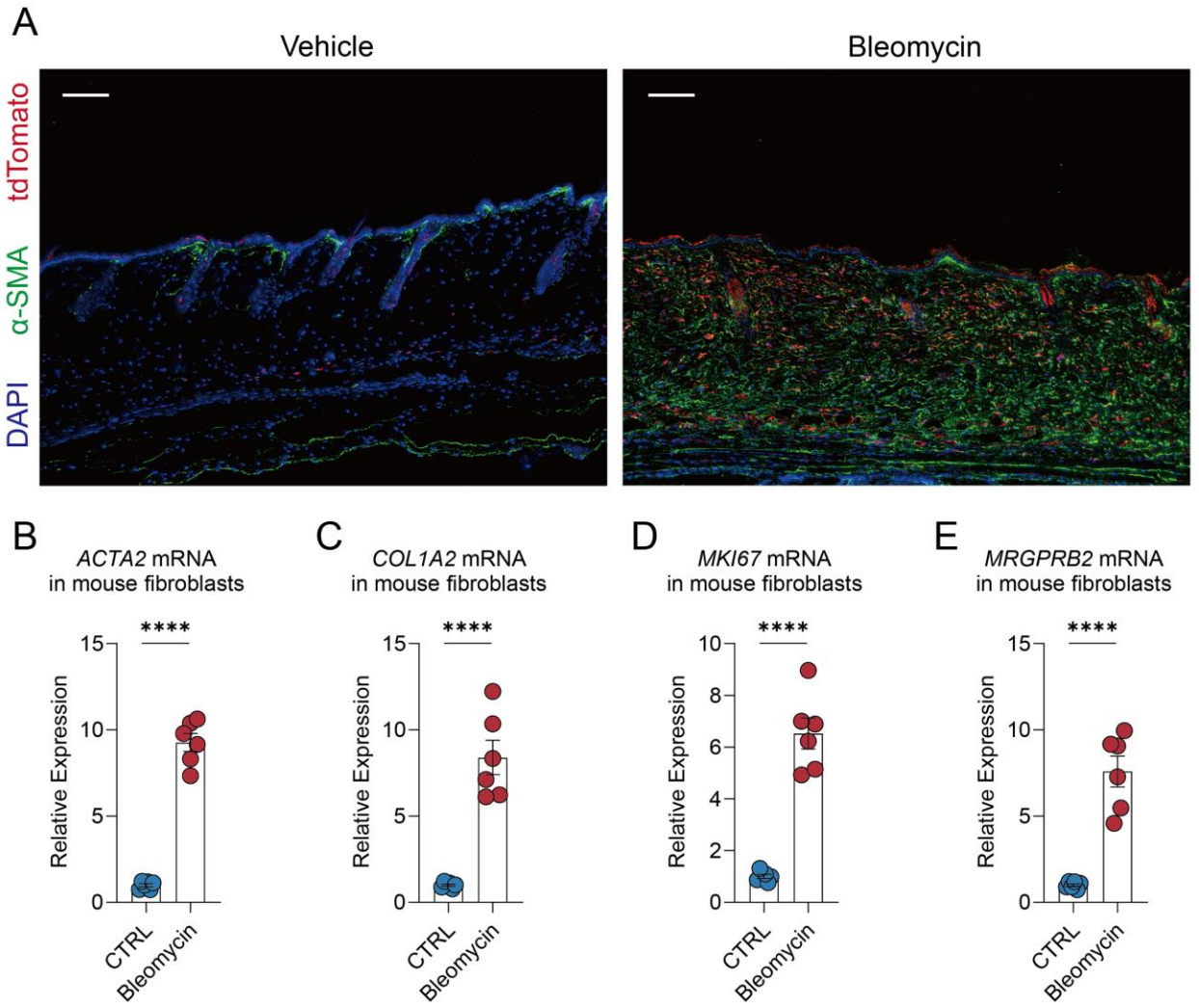

Figure S17. *MRGPRB2*⁺ cells contribute to myofibroblast population in bleomycin-induced fibrosis.
(A) Representative immunofluorescence images for α-SMA (green), DAPI (blue), and tdTomato (red) in control and bleomycin-treated mouse skin utilizing *MRGPRB2*^{cre}*;Ai9* mice. n = 6 per group. Scale bar = 100 μm.
(B–E) RT-qPCR analysis of dermal fibroblasts isolated from control and bleomycin-treated mice, showing significant upregulation of *ACTA2* (B), *COL1A2* (C), *MKI67* (D), and *MRGPRB2* (E) following bleomycin treatment (n = 6 per group). Student's *t*-test.
Data are shown as mean ± SEM. ****$P < 0.001$.